

Long time simulations of granular hydrodynamics : instabilities and attractors

Srikant Marakani and Gene F. Mazenko,
The James Franck Institute and Department of Physics,
University of Chicago,
Chicago, Illinois 60637, USA.

November 10, 2018

Abstract

Using a hydrodynamic model of granular flows, we present very long time simulations of a granular fluid in two dimensions without gravity and with periodic boundary conditions in a square domain. Depending upon the values of the viscosity, thermal conductivity and dissipation, we find for intermediate times a metastable clustering state. For longer times the system is attracted to either a shear band or a vortex state. Our results are in general agreement with molecular dynamics simulations.

1 Introduction

Granular materials are an economically important and physically interesting system[1]. These materials are dissipative in nature and have complex behaviour and exhibit very interesting phenomena such as clustering[2] and *Maxwell Demon* effects[3]. The fact that the behaviour of these materials is in many ways similar to conventional fluids was noted very early and a hydrodynamic approach to them was developed heuristically by Haff[4] and Jenkins and Savage[5]. More recently a similar hydrodynamic approach has been developed by considering a Chapman-Enskog expansion of the Boltzmann equation for a granular system by Brey, Dufty, Kim and Santos[6, 7].

In this paper, we study a modification of the Haff equations by Hill and Mazenko[8] which enabled the use of the hydrodynamic equations to be extended to systems with clustering instabilities. This model has the advantage of avoiding inelastic collapse and of being able to be simulated efficiently on a computer. Further, it was also shown by Hill and Mazenko[9] that these hydrodynamic equations form a well-defined system of equations under a range of circumstances. It therefore also suggests the possibility that the nonlinear hydrodynamical approach is applicable outside the conventional regime of low densities. We investigate this model in detail and show that it exhibits many of the features found from molecular dynamic simulations[10, 11]. Some new features not previously described have also been found and it should be possible to check if these features also exist in conventional molecular dynamic simulations.

2 The Hydrodynamic Equations

In this paper, we used the hydrodynamic equations postulated by Haff[4]. They are essentially the Navier-Stokes equations with the transport coefficients being dependent upon the density and the granular temperature[12] and with an extra dissipation term due to the inelastic nature of the particles. Written out fully, the equations are[8]

$$\frac{\partial \rho}{\partial t} = -\nabla_i(\rho u_i) \quad (1)$$

$$\frac{\partial(\rho u_i)}{\partial t} = -\nabla_j[(\rho T + P_f)\delta_{ij} + \rho u_i u_j - \eta_{ijkl}\rho T^{\frac{1}{2}}\nabla_k u_l] \quad (2)$$

$$\frac{\partial T}{\partial t} = -u_i \nabla_i T - T \nabla_i u_i + \frac{1}{\rho} \kappa \nabla_i (T^{\frac{1}{2}} \nabla_i T) + \quad (3)$$

$$\eta_{ijkl} T^{\frac{1}{2}} \nabla_i u_j \nabla_k u_l - \gamma T^{\frac{3}{2}}$$

where sums over repeated indices is implied, ρ stands for the density, u_i for the components of the velocity, t for the time, T for the granular temperature[13], P_f for the pressure due to the free energy, η for the viscosity tensor, κ for the thermal conductivity and γ for the thermal dissipation coefficient. The derivation of these equations is discussed in detail in Haff[4][14]. We use the usual form

$$\eta_{ijkl} = \eta(\delta_{ik}\delta_{jl} + \delta_{il}\delta_{jk}) + \chi\delta_{ij}\delta_{kl} \quad (4)$$

for the viscosity tensor where η and χ stand for the shear and bulk viscosities respectively.

Similar equations can be derived[6, 15] by performing a Chapman-Enskog expansion of the Boltzmann equations for an inelastic hard sphere model about the homogeneous state. These equations are rather similar except for some scaling differences for γ and η and an extra term involving the density gradient. The pressure term in this model is just of the ideal gas form. The viscosity also has a very simple form with the bulk viscosity being equal to the shear viscosity.

Following Hill and Mazenko[8], we simulated the Haff equations with a pressure term which reflects the interactions between the grains.

3 The simulation of the hydrodynamic equations

The Haff equations were simulated with the same basic algorithm as in Hill and Mazenko[8]. The algorithm was improved with the use of a superior adaptive step technique which speeded up the simulations significantly without loss of accuracy. As in Hill and Mazenko[8], the pressure term is chosen in the model to account for the excluded volume effects in the granular fluid. The pressure, is, as usual, related to the free energy density f by $p_f = \rho \frac{\partial f}{\partial \rho} - f$. The interaction part of the free energy density used for this purpose was chosen to be of the form

$$f(\rho) = K(\rho - \rho_c)^\alpha \Theta(\rho - \rho_c) \quad (5)$$

where Θ is the step function and ρ_c is the packing density. In Hill and Mazenko[8], $\alpha = 2$. This free energy corresponds to particles which behave roughly like stiff springs with regard to compression. In our work, we chose $\alpha = 10$ to preserve the continuity of the higher derivatives of $f(\rho)$ which enables the higher order accuracy of the fourth-order Runge-Kutta method to be exploited. This roughly corresponds to particles with a very thin soft exterior and a hard interior. In the simulations, it is however not difficult to verify that the precise form of this free energy density is not important as long as the interaction is stiff enough. The large value of α permits a much smaller range of densities above the packing density. The value $K = 4 \times 10^4$ was chosen in Hill and Mazenko[8] while we chose $K = 4 \times 10^{16}$ to adjust for the larger value of α .

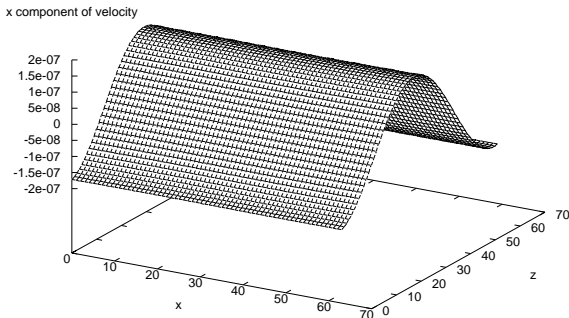


Figure 1: The x component of the velocity for a system that has been attracted to a final shear state ($\eta = 5, \gamma = 1, t = 10^9$).

We also added a fictional term to the free energy density

$$f_v = A\Theta(\rho_v - \rho)(\rho - \rho_v)^{10} \quad (6)$$

where $\rho_v = 10^{-3}, A = 10^{30}$. This contribution to the pressure prevents areas of extremely low density from being produced since these cause numerical instabilities.

4 Observations

The units used in this paper are the same as in Ref. [8]. The initial conditions chosen for most of the simulations were a uniform density half the packing density ($\rho_c = 0.2$), random uniformly distributed initial velocities in the range $[-1, 1]$ for each component (ensuring that the initial center of mass velocity was zero) and a uniform granular temperature of 1. These conditions were chosen for their relative simplicity. The precise random configuration of velocities was seen in some cases to matter significantly in the subsequent dynamical evolution of the system including the form of the final state achieved. The dynamical equations were solved numerically on a grid in space where the lattice spacing was chosen to be 0.9 for most simulations, a value which was verified to provide good accuracy for the values of viscosity that we used. The densities were stored at the intersection points of the

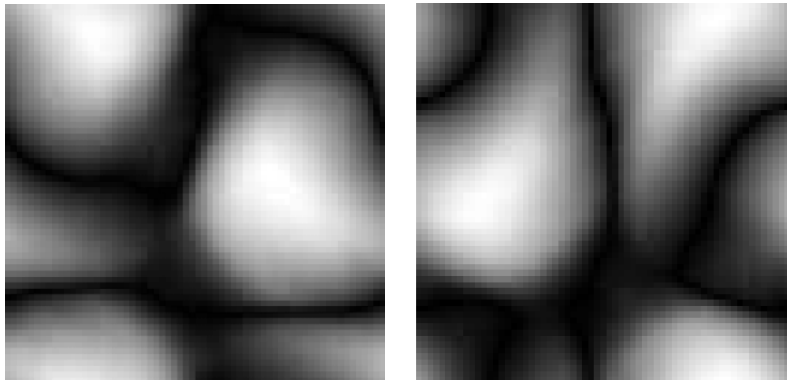


Figure 2: The x and z velocity distributions for a vortex state seen as a greyscale map (intensity of white proportional to absolute velocity, $\eta = 9, \gamma = 11, t = 10^9$). For the x velocity distribution shown in the left image, the large white region on the right has a negative velocity while for the z velocity distribution shown in the right, the large white region on the left has a positive velocity.

grid while the velocities were stored at the mid-points of the lines between the intersections (x -components on the lines perpendicular to the x -axis and the z -components on the lines perpendicular to the z -axis). The upwind technique was then used to determine which velocity corresponded to which density. The method is described in detail in Ref. [16]. The fourth order Runge-Kutta method was used for the time evolution and an adaptive time step based on the estimated error from a single time step and two steps of half the size used to control the error and speed up the simulation.

There are a number of parameters in the model. It is important to realize that the viscosity sets the major length scale in the problem and larger viscosities enable us to use larger lattice spacings without introducing large numerical errors. For some low viscosity simulations, we have used smaller lattice spacings.

In contrast to the work of McNamara and Young[17], our simulations have been run long enough to access the final attracting states. The simulations have also been performed for a wide range of values in parameter space. These final attracting states have been discussed in some detail in Soto and Mareschal[18]. There is the well known homogenous cooling state (HCS) with uniformly decreasing average velocity and temperature, and no structure formation. There is the shear band configuration[18] with the velocity field

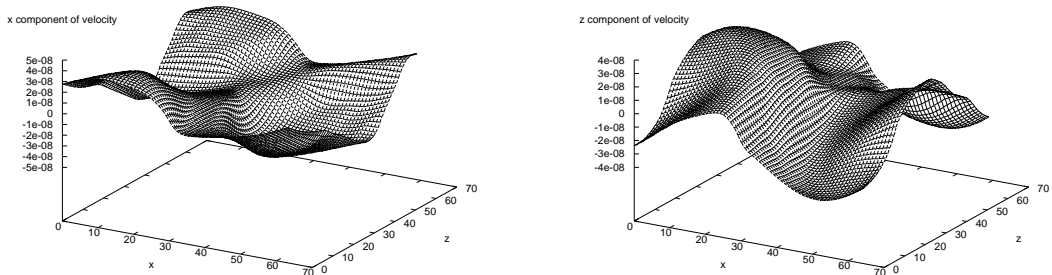


Figure 3: The x and z velocity distributions for a system in the vortex state ($\eta = 9, \gamma = 11, t = 10^9$).

taking on the form $\mathbf{v} = v_0(t) \cos(2\pi x/L) \hat{\mathbf{z}}$ or $\mathbf{v} = v_0(t) \cos(2\pi z/L) \hat{\mathbf{x}}$ where $\hat{\mathbf{z}}$ and $\hat{\mathbf{x}}$ are the unit vectors in the z and x directions respectively and L is the size of the domain. An example of the distribution of the x component of the velocity distribution in a shear band state in the x direction is shown in figure 1.

The final type of attractor is a cyclical one with features similar to a vortex structure. If we define

$$\gamma = \sqrt{\frac{E(t)}{E(0)}} \quad (7)$$

where $E(t) = \langle \rho u^2 + T \rangle$ stands for the energy at time t and consider the rescaled velocities $v = u/\gamma$ and differentially rescaled time

$$ds = \gamma dt \quad (8)$$

we find that v is a periodic function of s . A greyscale map of the x and z components of the velocity distribution at a point in the cycle is shown in figure 2. Seen this way, the cyclical structure looks like two tadpole-like structures moving much like two shear bands. This seems to be related to the state with two counter-rotating vortices found in the nonlinear analysis of Soto and Mareschal[18] where the velocity is dominated by the $k_x = \frac{2\pi}{L}, k_z = \frac{2\pi}{L}$ mode in Fourier space. Another view of the velocity distribution is shown in figure 3. The density distribution at various times in the cycle is shown in figure 4.

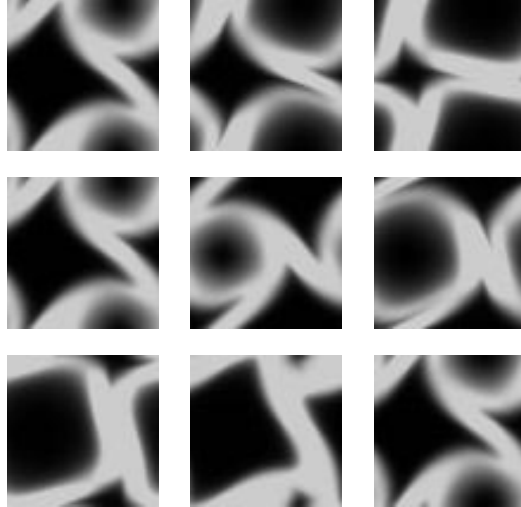


Figure 4: The density distribution for the vortex state (density is proportional to the intensity of white in the figure). The time goes from left to right and top to bottom, with the values being $t = 1.734 \times 10^8, 1.842 \times 10^8, 2.197 \times 10^8, 2.895 \times 10^8, 3.779 \times 10^8, 4.545 \times 10^8, 5.437 \times 10^8, 7.252 \times 10^8$ and 9.391×10^8 .

We also find, as in past studies[17, 10, 11], an intermediate clustering state which is metastable. However, which particular final attracting state is chosen seems to depend on many criteria including the starting distribution of velocities. The homogeneous cooling state is chosen by the system when the dissipation is low[18]. However, if the system size is large enough, any dissipation will make the homogeneous cooling state unstable[18]. Soto and Mareschal[18] carried out a non-linear stability analysis for the shearing and vortex states and found a criterion for the stability of the states provided the deviations from the homogeneous cooling state were small. The criterion is relatively simple but is accurate only when the state does not deviate too much from the homogeneous cooling state. In our simulations, shear bands were mostly observed but some vortex states were also observed even with the same parameters but different system sizes or initial conditions. For simulations with $\kappa = 10, \chi = 1$, the vortex attracting state was achieved for $(\eta, \gamma) = (7, 7), (7, 15), (9, 11)$ and $(9, 19)$ in one of the runs (since the final state does depend on the initial conditions, it occurred for different values of the parameters in other runs). It is also interesting to note that the velocity

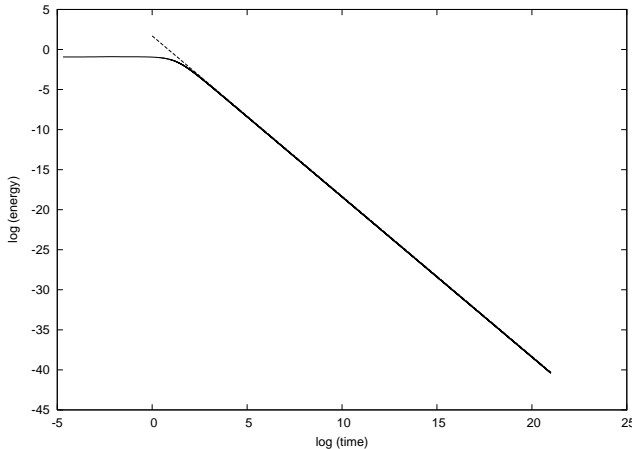


Figure 5: A plot of $\log E$ versus $\log t$ for a system that never leaves the HCS ($\eta = 25, \gamma = 0.1$). A line with slope -2 is drawn for reference purposes.

field is always the first to go to the attracting state with the other fields following much later.

We can be somewhat more quantitative if we look at the evolution of the energy (defined as $E = \langle \rho(\frac{1}{2}u^2 + T) \rangle$) and the granular thermal energy (defined as $E_T = \langle \rho T \rangle$) with time[17, 10, 11]. It is well known that in the HCS, the energy evolves as

$$E(t) = \frac{E(0)}{(1 + t/t_0)^2} \quad (9)$$

so that at large times, the slope of a log-log plot of energy with respect to time has a slope of -2. We show this plot for a system which never leaves the HCS in figure 5. The plot for a system which has the clustering instability is shown in figure 6. We see that during the clustering instability, the rate of decrease of energy is reduced. Some studies[11] indicate that the rate of decrease of the energy goes as $E \sim t^{-1}$ during this metastable phase but we find that the relation depends on the value of the parameters. The plot for a system which has the clustering instability and which settles into the vortex state is shown in figure 7. The reduction in the rate of decrease of energy in the clustering phase is similar to that of a system that finally goes into a shear band state but the cyclical nature of the final state is clearly seen in this plot. The average slope of the plot in the final state is still -2.

The evolution of the granular thermal energy $E_T = \langle \rho T \rangle$ has a similar

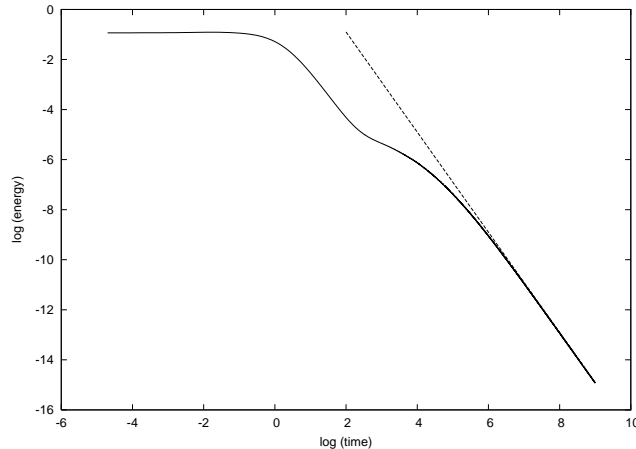


Figure 6: A plot of $\log E$ versus $\log t$ for a system that has a clustering instability and which finally settles into a shear band state ($\eta = 5, \gamma = 1$). A line with slope -2 is drawn for reference purposes.

behaviour. The corresponding log-log plots are shown in figures 8, 9 and 10. It is very interesting to note that the granular thermal energy E_T does go as t^{-1} for the initial evolution of the clustering state and this does seem to be independent of the parameters. This result might be related to the one found by Xiaobo et al[11] and Miller and Luding[19] where the kinetic energy decays as t^{-1} in molecular dynamics simulations. The slope of the plots, discussed in some detail in Hill and Mazenko[8], $V_E = \frac{d \log E_T}{d \log t}$, is another interesting quantity. Examples of the behaviour of V_E are shown for several values of the parameters in figures 11, 12, 13 and 14 respectively. It is interesting to note that in systems where there is a clustering instability, V_E has large fluctuations in the later part of the evolution of this phase.

Since the energy behaves as (9) in the HCS and the system is initially in the HCS, we have

$$V_E = -\frac{2}{1 + t_0/t} \quad (10)$$

Since t_0 is relatively small (of order 1), V_E should rapidly decrease from 0 to -2 if the system stays in the HCS. Any increase in V_E signals a departure from the HCS and we can hence identify the time at which V_E reaches a minimum as the time the system begins to depart from the HCS. We define this time to be t_E . It was found earlier[8] that t_E [20] followed a power law with respect to γ , that is $t_E \sim \gamma^\mu$. This result cannot hold for all γ since, for a given

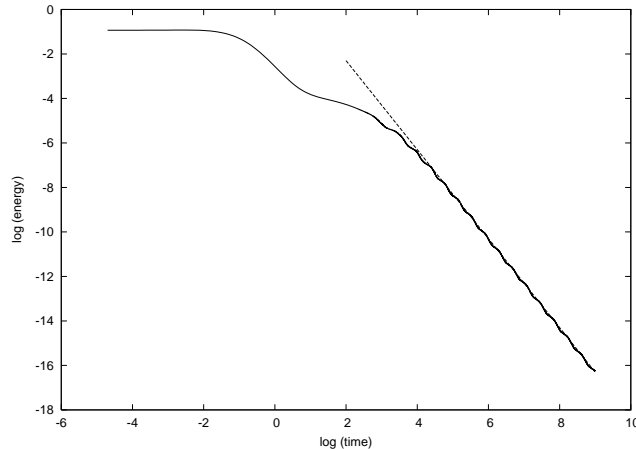


Figure 7: A plot of $\log E$ versus $\log t$ for a system that has a clustering instability and which finally settles into a vortex state ($\eta = 9, \gamma = 11$).

system size, there is a finite cutoff γ_c below which the system never leaves the HCS. However, for γ well above this value (which is generally much less than 1 except for high viscosities), we find a power law relation for several values of η ($\chi = 1, \kappa = 10$ being held fixed) with the exponent μ being in the range $[-1.5, -1.4]$. Examples of the power law behavior for several values of the viscosities are shown in figure 15. .

Another quantity of interest which has been analysed earlier in the literature^[17] is the ratio of the thermal energy to the kinetic energy E_T/E_k . For a vortex state, the behaviour is interesting in that this ratio oscillates about a fixed value as seen in figure 16. This is another example of the cyclical behaviour of this attractor. For a shear state, the ratio approaches a constant value asymptotically as seen in figure 17.

We now look at the clustering instability a bit more closely so as to identify clearly when it occurs. Since phase separation can be due to the clustering instability or a result of the velocity gradients in an attracting state, we have to distinguish between these two. To do so, we characterize phase separation as having occurred if the rms fluctuation in the density is above 0.3 and the system has reached the packing density at at least one point. We call the time at which this first occurs as t_{phase} . We then identify the time t_{final} at which the system has reached its final state. The main feature of the shear band state is the picking of one direction in which the bands occur. The result of this is a dominance of kinetic energy in that

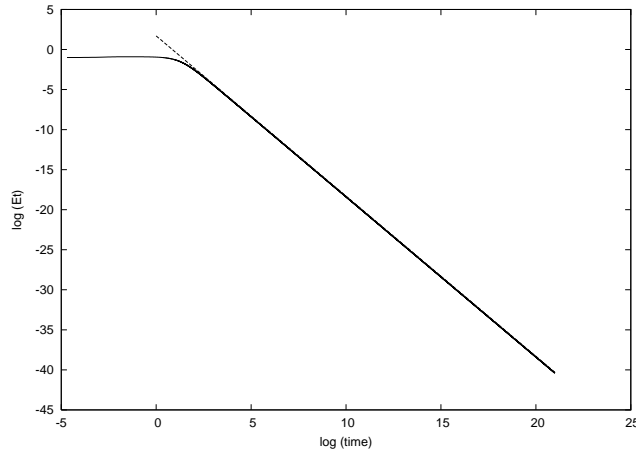


Figure 8: A plot of $\log E_T$ versus $\log t$ for a system that never leaves the HCS ($\eta = 25, \gamma = 0.1$). A line with slope -2 is drawn for reference purposes.

direction. Hence, for a shear band state, we identify t_{final} as the first time at which the kinetic energy in one direction dominates the kinetic energy in the other direction by a factor of 1000, that is the first time when $\frac{\langle \rho u_x^2 \rangle}{\langle \rho u_y^2 \rangle} > 1000$ or when $\frac{\langle \rho u_y^2 \rangle}{\langle \rho u_x^2 \rangle} > 1000$. A similar criterion is used to identify the shearing state in McNamara and Young[17]. For a vortex state, we indentify t_{final} as the time at which the oscillations in E_T/E_k start. If $t_{phase} < t_{final}$ we claim that the phase separation is a result of the clustering instability. Using this criterion, the phase diagram for the clustering instability is shown in figure 18.

5 Summary and Conclusions

To summarize, we have used a hydrodynamic model of granular dynamics to simulate the cooling of a granular gas with no external field and with periodic boundary conditions over a large region of parameter space. We have found that the results of simulations using this model are in broad agreement with molecular dynamic simulations of the same phenomenon. We find that the system is attracted to one of three final states - the homogeneous cooling state, the shear band state or a vortex state. The HCS is the final state only if the system is small and the dissipation is very low while the shear band or vortex states result when the dissipation is high with the exact criterion

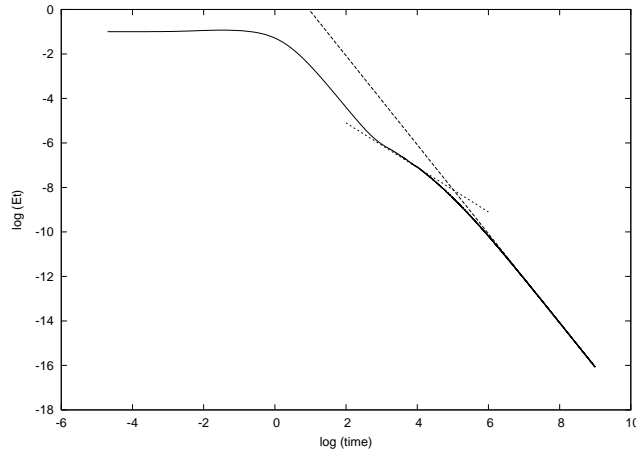


Figure 9: A plot of $\log E_T$ versus $\log t$ for a system that has a clustering instability and which finally settles into a shear band state ($\eta = 5, \gamma = 1$). Lines with slope -1 and -2 are drawn for reference purposes.

for the selection of the state unknown though it has been found to depend on the initial state of the system. We have also found a phase diagram for the clustering instability in this model and have confirmed the result in Hill and Mazenko[8] that the time taken to depart from the homogeneous cooling state follows a power law with respect to the dissipation coefficient (for high enough dissipation) over a much larger region of parameter space. It should be possible to check this result with molecular dynamic simulations.

Acknowledgements

We thank Scott Hill for his help and one of us, Srikant Marakani, would like to thank Mrs. Lalitha Chandrasekhar for providing the fellowship that enabled him to pursue this research. This work was also supported by the Materials Science and Engineering Center through grant No. NSF DMR-9808595.

References

- [1] J. Duran, *Sands, powders and grains : an introduction to the physics of granular materials*, Springer Verlag, 1999.

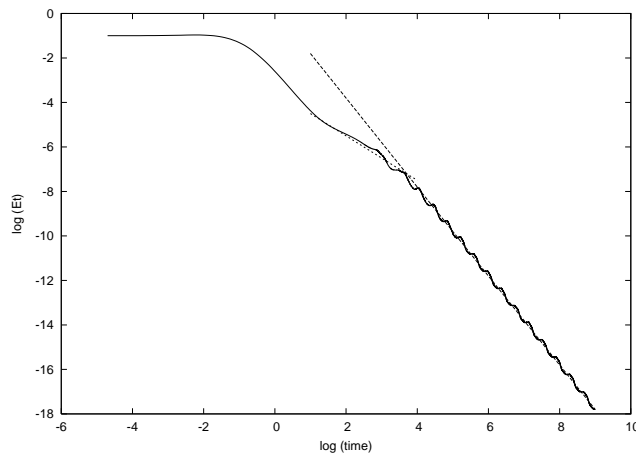


Figure 10: A plot of $\log E_T$ versus $\log t$ for a system that has a clustering instability and which finally settles into a vortex state ($\eta = 9, \gamma = 11$). Lines with slope -1 and -2 are drawn for reference purposes.

- [2] I. Goldhirsch and G. Zanetti, Phys. Rev. Lett. **70**, 1619 (1993).
- [3] J. Eggers, Phys. Rev. Lett. **83**, 5322 (1999).
- [4] P. K. Haff, J. Fluid Mech. **134**, 401 (1983).
- [5] J. T. Jenkins and S. B. Savage, J. Fluid Mech. **130**, 187 (1983).
- [6] J. J. Brey, J. W. Dufty, C. S. Kim, and A. Santos, Phys. Rev. E **58**, 4638 (1998).
- [7] J. W. Dufty and J. J. Brey, Phys. Rev. E **68**, 030302 (2002).
- [8] S. A. Hill and G. F. Mazenko, Phys. Rev. E **67**, 063102 (2003).
- [9] S. Hill and G. F. Mazenko, Phys. Rev. E **63**, 031303 (2001).
- [10] S. Luding and H. J. Herrmann, Chaos **9**, 673 (1999).
- [11] X. Nie, E. Ben-Naim, and S. Chen, Phys. Rev. Lett. **89**, 204301 (2002).
- [12] The thermal temperature is irrelevant for granular flows since the thermal energy scale $k_B T$ is much less than the other energy scales.
- [13] In this model, the granular temperature T is an independent variable.

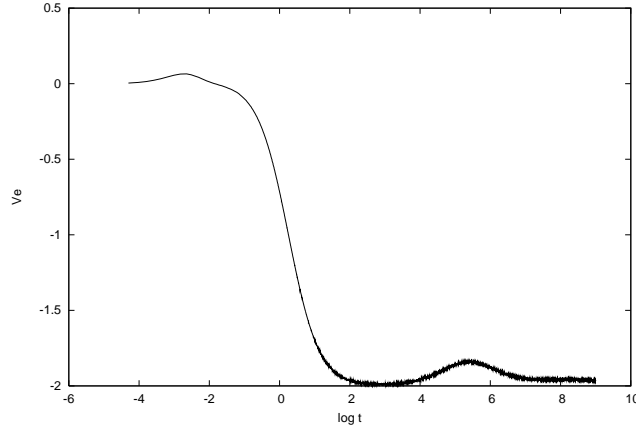


Figure 11: V_E versus time for $\eta = 25, \chi = 1, \gamma = 1, \kappa = 10$. This system goes directly to the shear state without a clustering instability.

- [14] See also Hill and Mazenko[9] for a different derivation which features the role of a driving free energy.
- [15] J. J. Brey and D. Cubero, Hydrodynamics and transport coefficients of granular gases, in *Granular Gases*, edited by S. Luding and T. Poeschel, Springer Verlag, 2001.
- [16] S. A. Hill, *Clustering in Granular Gases : A Hydrodynamic Simulation*, PhD thesis, University of Chicago, 2003.
- [17] S. McNamara and W. R. Young, Phys. Rev. E **53**, 5089 (1996).
- [18] R. Soto, M. Mareschal, and M. M. Mansour, Phys. Rev. E **62**, 3836 (2000).
- [19] S. Miller and S. Luding, Phys. Rev. E **69**, 031305 (2004).
- [20] The quantity used there was $\frac{d\log\langle T \rangle}{d\log t}$ rather than V_E . This does not produce any significant change in the results. We use V_E since E_T is a better behaved quantity compared to the local temperature which has large fluctuations with respect to the average when the local density is low.

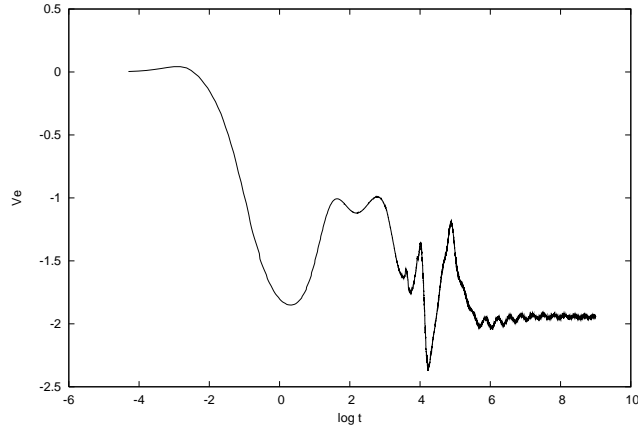


Figure 12: V_E versus time for $\eta = 25, \chi = 1, \gamma = 19, \kappa = 10$. This state goes finally to the shear state but only after a clustering instability phase.

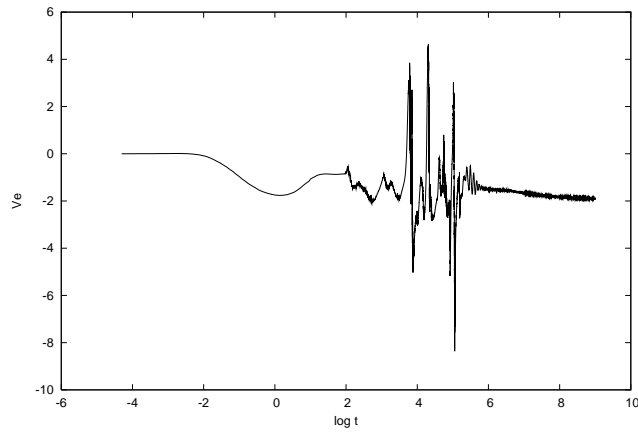


Figure 13: V_E versus time for $\eta = 7, \chi = 1, \gamma = 19, \kappa = 10$. This state goes finally to the shear state but only after a strong clustering instability phase.

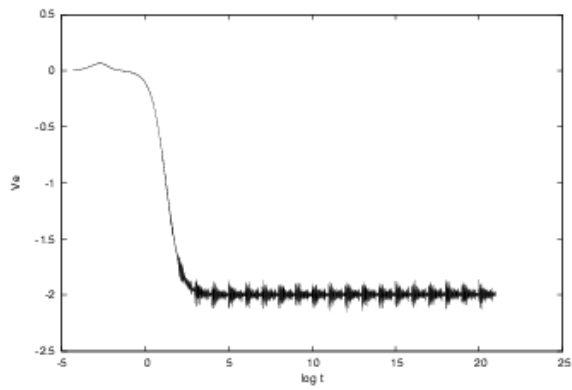


Figure 14: The derivative of the logarithm of the thermal energy with respect to the logarithm of the time for a system with $\eta = 25$, $\chi = 1$, $\kappa = 10$, $\gamma = 0.1$ which does not exit the HCS. We see that the derivative settles to -2 and does not change. The small deviations from -2 seem to be due to numerical errors.

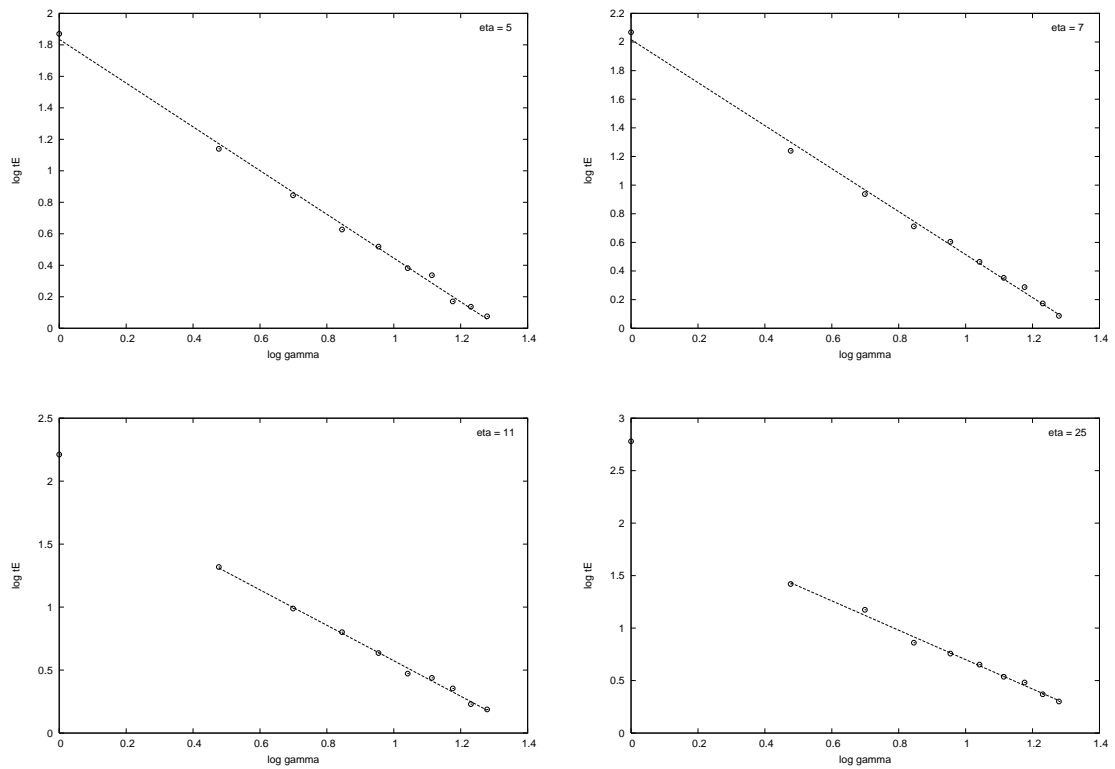


Figure 15: The power law $t_E = \gamma^\mu$ for $\eta = 5, 7, 11, 25$. Note that for $\eta = 11, 25$, we have to exclude the first point from the fit since it is too close to γ_c . The values for μ are $-1.39, -1.50, -1.41$ and -1.40 respectively.

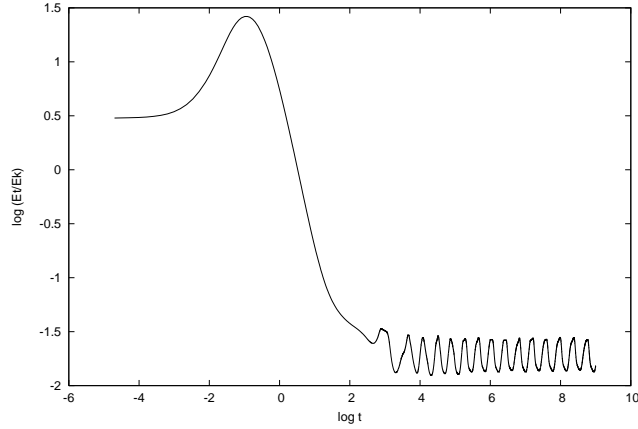


Figure 16: The ratio of the thermal to kinetic energy E_T/E_k for $\eta = 9, \gamma = 11, \chi = 1, \kappa = 10$ which goes to a final vortex state. Note that once the system reaches the vortex state, the ratio oscillates about a constant value.

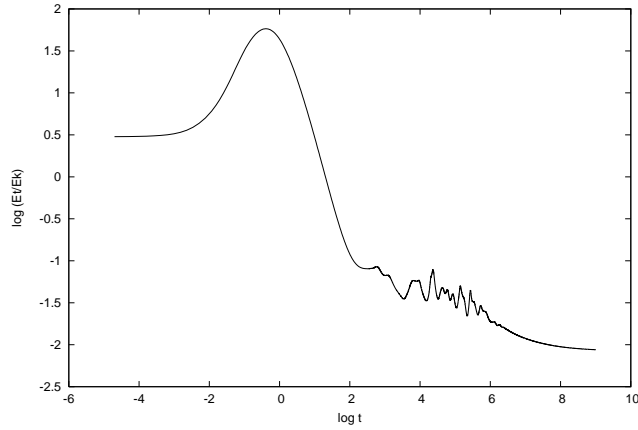


Figure 17: The ratio of the thermal to kinetic energy E_T/E_k for $\eta = 5, \gamma = 3, \chi = 1, \kappa = 10$ which goes to a final shear state. Note that once the system reaches the shear state, the ratio converges to a constant.

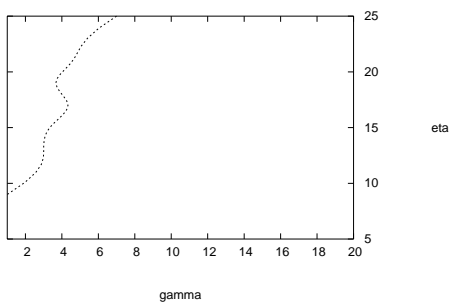


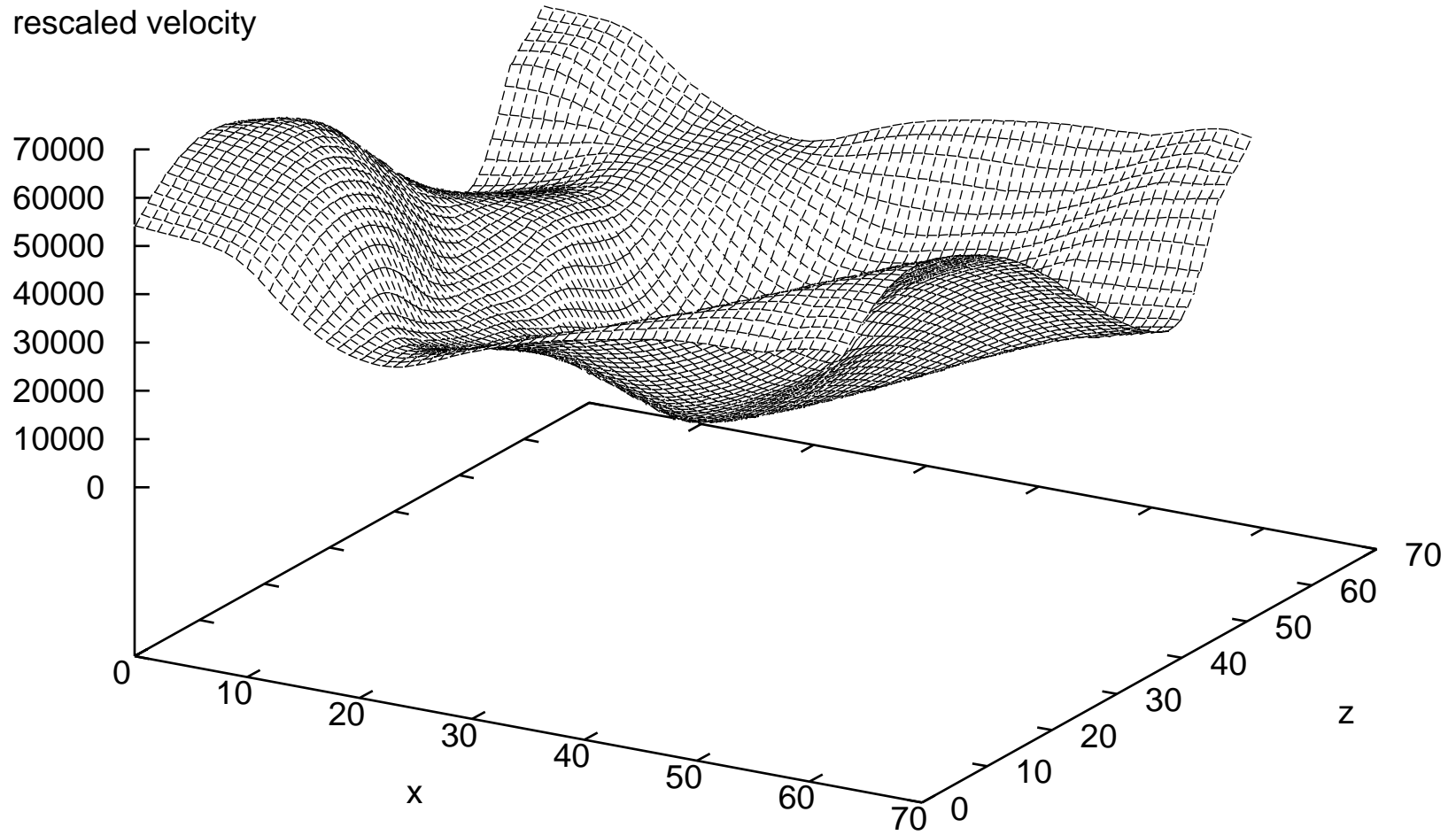
Figure 18: The phase diagram for the clustering instability. The values of the other parameters are $\chi = 1, \kappa = 10$. Clustering occurs for parameters to the right of the dashed line.

This figure "dlogEtdlogt_eta25_gam01_kappa10.png" is available in "png" format fr

<http://arxiv.org/ps/cond-mat/0406572v1>

Rescaled x component of velocity for $\eta=7$, $\chi=1$, $\kappa=10$

rescaled velocity



Rescaled z component of velocity for $\eta=7$, $\chi=1$, $\kappa=10$

rescaled velocity

